The Natural Product 3',4',7,8- tetrahydroxyflavonoid Is a Potent BRD4-BD2 Inhibitor in Suppressing Acute Myeloid Leukemia

Jiao Li[1a], Wei Zou[2a], Koukou Yu[1], Bing Liu[1], Weifeng Liang[1], Lisha Wang[3], Yin Lu[2], Zequn Jiang[1], Aiyun Wang[2*], Jiapeng Zhu[1*]

1 School of Medicine & Holistic Integrative Medicine, Nanjing University of Chinese Medicine, Nanjing, Jiangsu, China.

2 Jiangsu Key Laboratory for Pharmacology and Safety Evaluation of Chinese Materia Medica, School of Pharmacy, Nanjing University of Chinese Medicine, Nanjing, Jiangsu, China.

3 Department of Medicinal Chemistry, PharmaBlock Sciences (Nanjing), Inc., 10 Xuefu Road, Nanjing 210032, China

[a] These authors contributed equally to this paper.

*Correspondence to: zhujiapeng@hotmail.com and wangaiyun@njucm.edu.cn.

ABSTRACT

Background and Purpose: Bromodomain-containing protein 4 (BRD4) binds acetylated lysine residues on the N-terminal tails of histones through two bromodomains (BD1 and BD2) to regulate gene transcription. Inhibiting one or both of the bromodomains results in different phenotypes, suggesting BD1 and BD2 may have different functions. Here we report the characterization of a natural product 3',4',7,8-tetrahydroxyflavonoid as a new and potent BRD4 inhibitor with anti-cancer activities *in vitro* and *in vivo*.

Experimental Approach: AlphaScreen assays were performed to evaluate the inhibitory activities of 3',4',7,8-tetrahydroxyflavonoid against the bromodomains. Crystal structures of the compound bound to BRD4-BD1 or BD2 were solved to reveal key binding features. MV4-11 *in vitro* cell culture model and xenograft mouse models were used to examine the compound's anti-cancer activities. Western blotting, Immunofluorescence staining and RT-PCR were used to investigate the mechanism(s) of the compound in suppressing MV4-11 cell and tumor growth.

Key Results: 3',4',7,8-tetrahydroxyflavonoid is ~100-fold more selective for BRD4-BD2 (IC_{50}=204 nM) than BD1. Co-crystal structures show 3',4',7,8-tetrahydroxyflavonoid establishes more interactions in BRD4-BD2 acetylated lysine binding pocket than BD1. Consistent with a selective and high affinity with BRD4 bromodomains, 3',4',7,8-tetrahydroxyflavonoid treatment inhibited MV4-11 cell growth and reduced AML tumor growth *in vitro* and *in vivo*,

respectively.

Conclusion and Implications: Our data suggest 3',4',7,8-tetrahydroxyflavonoid as a potent selective inhibitor of BRD4-BD2 with a novel chemical scaffold. Given its distinct chemical structure from current BRD4 inhibitors, this compound may open the door for a novel class of BRD4 inhibitors by serving as a lead compound.

Abbreviations

BRD4, bromodomain-containing protein 4; KAc, acetylated lysine; **3478**, 3',4',7,8-tetrahydroxyflavonoid; BD1, bromodomain 1; BD2, bromodomain 2; IC_{50}, half maximal inhibitory concentration; MV4-11, homo sapiens myelomonocytic biphenotypic leukemia cell line; AML, acute myeloid leukemia; c-Myc, chromosome Myc proto-oncogene protein.

1 INTRODUCTION

Bromodomain-containing proteins (BRDs) recognize acetylated lysine (KAc) residues on the N-terminal tails of histones to restructure chromatin and regulate transcription (Filippakopoulos & Knapp, 2014; Filippakopoulos et al., 2010). In the human proteome, there are 61 bromodomains located in 46 proteins that can be classified into eight families, one of which is the Bromodomain and Extra C-terminal domain (BET) family (Muller, Filippakopoulos & Knapp, 2011). Bromodomain-containing protein 4 (BRD4), a member of the BET family proteins, recruits transcriptional elongation factor complexes (P-TEFb) and facilitates RNA polymerase II-mediated transcription in eukaryotes (Filippakopoulos et al., 2010; Shin & Bayarsaihan, 2017).

BET proteins play an important role in pathogenesis including cancer and immune diseases due to their ability in modulating gene expression. To date, BRD4 is the most extensively studied BET family protein and has attracted great interest as a drug target. As other members of the BET family (BRD2, BRD3 and the testis-ovary specific BRDT), BRD4 has two tandem bromodomains (BD1 and BD2) and an extra C-terminal domain (ET) with a high sequence conservation through evolution (Filippakopoulos et al., 2012). Both BRD4-BD1 and BD2 interact with acetylated lysine residues in histone and non-histone proteins to regulate a variety of cellular process including transcription, DNA replication, cell cycle progression and others. BD1 and BD2 have been reported to recognize distinct sets of acetylated lysines and may exert different function through transcriptional regulation (Wang et al., 2019). BD1 preferentially binds acetylated lysines 5 and 8 of histone H4 tail peptides, while BD2 has more affinity for acetylated lysines 18 and 23 of histone H3 tail peptides (Morinière et al., 2009). The same bromodomains, BD1 or BD2, are more conserved across the BET family than different bromodomains in the same protein (Sheppard et al., 2020). For example, the sequence of BRD4-BD1 is more similar with BRD2-BD1 than BRD4-BD2. Thus it is easier to design bromodomain-selective inhibitors than protein-selective inhibitors. Inhibitors that bind BD1 and BD2 with equal affinities (pan-BET inhibitors) are dose-limiting toxic, which cause a reduced number of thrombocytes in the blood (thrombocytopenia) and symptoms of gastrointestinal toxicity (Amorim et al., 2016; Piha-Paul et al., 2019). In contrast, ABBV-744, a potent and selective inhibitor of the BD2 of BET family proteins showed

anti-proliferative activity in cell lines of acute myeloid leukemia and prostate cancer with fewer platelet and gastrointestinal toxicities (Faivre et al., 2020). A recent study suggested that BD1 inhibitors behaved the same as pan-BET inhibitors in cancer models, whereas BD2 inhibitors were predominantly effective in models of inflammatory and autoimmune diseases (Gilan et al., 2020).

Most of the reported BRD4 inhibitors are derived from several core chemical scaffolds including azepines, 3,5-dimethylisoxazoles, pyridones, triazolopyrazines, tetrahydroquinolines , 4-acyl pyrroles and 2-thiazolidinones (Liu et al., 2017). Here, we report 3',4',7,8- tetrahydroxyflavonoid (**3478**), a natural product that exists in the heartwood of *Acacia burkittii* and *Acaciaacuminata*(Grace, Wilsonb, Kandil, Dimitriadis & Coates, 2009), as a new inhibitor of BRD4 with a novel chemical scaffold. Natural products play an important role in drug discovery, especially in cancer treatments. They exhibit vast chemical diversity, distinct chemical scaffolds and high degrees of stereochemistry that enable them to provide hits even against difficult screening targets, such as protein-protein interactions (Drewry & Macarron, 2010). The additional advantage of natural products is their "metabolite-likeness" property that enables cell permissibility (Hert, Irwin, Laggner, Keiser & Shoichet, 2009). In this study, we provide both structural and functional studies to demonstrate that **3478** is a potent selective inhibitor of BRD4-BD2 with a novel chemical scaffold and new binding mode to BRD4 bromodomains, and by suppressing Myc expression, **3478** significantly reduced the human acute myeloid leukemia (AML) MV4-11 cell growth *in vitro* and xenografted tumor growth in mice without affecting body weight.

These data suggest **3478** can be further explored as a novel anti-cancer lead compound.

2 METHODS

2.1 Materials

3478 was purchased from BIOSYNTH® Carbosynth Ltd (Compton, UK). The pan-BET inhibitor JQ1 was from Changchun Sanbang Pharmaceutical Technology (Changchun, China). The MV4-11 cell line was a kind gift from Professor Tao Lu, China Pharmaceutical University. The A549 and HepG2 cell lines were from American type culture collection (ATCC). The BALB/cJGPT-Foxn 1nu/Gpt mice were purchased from GemPharmatech Co., Ltd. (Nanjing, China). The primary anti-c-Myc antibody, primary anti-BRD4 antibody and secondary Goat Anti-Rabbit IgG H&L antibody were purchased from Abcam (Cambridge, UK).

2.2 AlphaScreen Compound–Protein Interaction Assay

The AlphaScreen assays were performed by Reaction Biology Corp. (Malvern PA, USA). Recombinant Human N-terminal Histagged BRD4 BD1 and BD2 were expressed in *E. coli*. The C-terminal-Biotinylated Histone H4 peptide (residues 1-21) was used as ligand in the assay. In each well of the reaction plate, a mixture of BRD4 BD1 or BD2 and one individual compound in a reaction buffer containing 50 mM HEPES, 100 mM NaCl, 0.05% CHAPS, 0.1% BSA, and 1.0% DMSO (pH7.5), was added and pre-incubated for 30 min. C-terminal-Biotinylated Histone H4 peptide was added to each well and incubated for 30 min at room temperature with gentle shaking.

Then streptavidin-coated donor beads and AlphaScreen Ni acceptor beads (PerkinElmer) were added and the plate was sealed and incubated in the dark for 60 mins. When excited by 680 nm laser, donor beads generated singlet oxygens, which diffused to acceptor beads and was converted to light signal between 520 and 620 nm that was recorded with an AlphaQuest®-HTS Microplate reader (PerkinElmer). IC_{50} values and curve fits were obtained using GraphPad Prism 7.0 (San Diego, CA, USA).

2.3 Anti-cancer Assays *in Vitro* and *in Vivo*

2.3.1 Cell proliferation assays

The human acute myelomonocytic leukemia cell line (MV4-11) was grown in Iscove's Modified Dulbecco's Medium (IMDM) (Gibco, Grand Island, USA). Human lung adenocarcinoma cell line (A549) and human liver carcinoma cell line (HepG2) were grown in Dulbecco's Modified Eagle Medium (DMEM) (Gibco, Grand Island, USA). Human gastric cancer cell line (MKN45) was grown in RPMI-1640 (Gibco, Grand Island, USA). All medium were supplemented with 10% Fetal Bovine Serum (FBS) (Gibco, Grand Island, USA) and 1% Penicillin/Streptomycin (Hyclone, Utah, USA). All cell lines were cultured and maintained in an atmosphere consisting of CO_2 (5%) and room air (95%) at 37 °C. To determine MV4-11 cell proliferation, approximately 1×10^4 MV4-11 cells were seeded into each well of a 96-well plate and cultivated in 100μL of culture media supplemented with 10% FBS. Then in each well different concentrations of **3478**, JQ1 (positive control) and DMSO (negative control)

were added. After 48 hours, 10μL of the Cell Counting Kit-8 (CCK8) solution (Beyotime, China) was added to each well and incubated for 1 hour. Cell densities were measured by a microplate reader (Biotek).

2.3.2 Apoptosis assay

FITC Annexin V Apoptosis Detection Kit I (BD Biosciences, USA) was used to measure the percentage of apoptotic cells. The exposure of phosphatidylserine on the extracellular side of the cell membrane was quantified by Annexin V-FITC/PI staining. MV4-11 cells were incubated with different concentrations of JQ1 and **3478** for 48 hours. The cells were harvested, washed twice with cold phosphate buffer saline (PBS) and incubated with 5μL Annexin V-FITC and 5μL PI at room temperature for 15 min in the dark. Binding buffer (500μL, 1X) was subsequently added to each tube and the cells were immediately analyzed using fluorescence-activated cell sorting (FACS) (BD Accuri C6, USA).

2.3.3 Construction of AML xenograft mice model and *in vivo* tumor suppression experiment

Male BALB/c nude mice aged six-week old and weighing 18-22g were purchased from GemPharmatech Co., Ltd. (Nanjing, China). The mice were housed (five per cage) under standard laboratory conditions ((22±2) °C, humidity (50±5)%, light /dark cycle 12/12h) and maintained in a specific pathogen-free facility. All mice were allowed free access to the normal chow diet and tap water. Ten mice were randomly chosen and reserved as the control group, which were orally administered with

0.1mL/10g 0.3% Carboxymethylcellulose Sodium (CMC-Na) once a day; the rest of mice were each injected with approximately $5x10^6$ MV4-11 cells into the right lower extremity and allowed two weeks to establish tumors. The mice were monitored daily for general health, and body weights were measured twice weekly. When the mean tumor volume reached 100 mm^3, the mice were randomly divided into four experimental groups (n=10): model group (orally administered with 0.1mL/10g 0.3% CMC-Na), JQ1 group (orally administered with 50mg/kg JQ1 daily), and **3478** groups (orally administered with 50mg/kg and 100mg/kg **3478** daily). JQ1 and **3478** were dissolved in 0.3% CMC-Na solution. The tumor size was measured with a vernier caliper twice a week and the tumor volume was calculated as 0.5×L×W×H, where L, W and H represent the longest dimension, widest dimension, and the highest dimension of the tumor, respectively. Relative tumor volumes were calculated as V_t/V_0 (V_t and V_0 represent the tumor size of the day of measurement and the day of initial treatment, respectively). Mice were weighed twice a week and considered dead when tumor volume reached 1000 mm^3 or the mice died during treatment. After four weeks of administration, mice were sacrificed by cervical dislocation and xenograft tumors were excised and stripped of non-tumor tissue and weighed. The tumors were bisected: one part was fixed in 10% formalin and paraffin-embedded for immunofluorescence staining; the other part was snap-frozen and stored in liquid nitrogen for Western blotting and quantitative PCR analysis.

All experimental protocols were approved by the Animal Care and Use Committee of Nanjing University of Chinese Medicine (Nanjing, China) and conducted under the

Guidelines for the Care and Use of Laboratory Animals (202005A024). Institutional and regional ethic committees approved all procedures above. Animal studies are reported in compliance with the ARRIVE guidelines (Kilkenny, Browne, Cuthill, Emerson & Altman, 2010) and with the recommendations made by the British Journal of Pharmacology.

2.3.4 Western blotting

Cell and tumor tissue homogenates were lysed in radioimmunoprecipitation assay buffer (Thermo Fisher Scientific, Waltham, MA, USA) containing protease and phosphatase inhibitors (Roche, Cat. No.: 04693116001, 04906837001) on ice for 30 min. After centrifugation at 14000 rpm for 5 min at 4 °C, the supernatant was collected and the protein concentration was determined using BCA assay. Western blotting was performed as previously described (Wei et al., 2017). Briefly, proteins were separated by sodium dodecyl sulphate-polyacrylamide gel electrophoresis and immunoblotted with antibodies against BRD4, c-Myc (Abcam, Cambridge, UK), and GAPDH (Bioworld, Visalia, CA, USA). The protein bands were visualized with enhanced chemiluminescence reagent (Biosharp, Wuhan, China) and the protein levels were quantified by scanning densitometry (Gel Doc-2000, Bio-Rad).

2.3.5 Immunofluorescence staining

Immunofluorescence staining was performed as described (Eriksson et al., 2002; Hosaka et al., 2013). Mice were sacrificed and tumor tissues were fixed in 4% PFA, dehydrated, and embedded in paraffin. Embedded samples were sectioned and 5 μm sections were immunostained with the following antibodies. Primary antibodies:

Anti-c-Myc antibody (Abcam, Cambridge, UK); secondary antibodies: Goat Anti-Rabbit IgG H&L (Abcam, Cambridge, UK). Nuclei were counterstained by Hoechst (Beyotime, Shanghai, China) at room temperature for 15 min. Pictures were captured with a fluorescence microscope (Zeiss, Jena, Germany).

2.3.6 Quantitative RT-PCR

SYBR green-based real time quantitative PCR was used to measure the mRNA transcriptional levels. Briefly, total cellular RNA from the lysates of transplanted tumors or cells was extracted with chloroform after addition of Trizol reagent (Thermo Fisher Scientific, Waltham, MA, USA). After precipitated with isopropanol, the RNA fraction was dissolved in DEPC-H_2O. An aliquot of 5μg RNA was reverse-transcribed into cDNA with a HiScript II QRT SuperMix for qPCR (+gDNA wiper) kit (Vazyme Biotech Co., Ltd, Nanjing, China). Quantitative RT-PCR was performed using a SYBR Green Master kit (Bio-Rad, USA). The primer pairs for RT-PCR are as follows: GAPDH (forward: 5'-GGTTGTCTCCTGCGACTTCA-3', reverse: 5'-TGGTCCAGGGTTTCTTACTCC-3'), c-Myc (forward: 5′-GGCTCCTGGCAAAAGGTCA-3′, reverse: 5′-CTGCTAGTTGTGCTGATGT-3′). Gene expression levels of the samples were calculated relative to the control using comparative CT method as follows: $\Delta\Delta CT = \Delta CT_{sample} - \Delta CT_{control}$, fold change = $2^{-\Delta\Delta CT}$. GAPDH expression was used as the internal control.

2.3.7 Statistical analysis

Except the data from mice (Section 2.3.3), all data were obtained from at least three

repeated experiments and are expressed as the MEAN ± SEM (standard error of the mean). Two-group comparisons were made by the unpaired Student's *t*-test, and multiple comparisons were analyzed by one-way analysis of variance (ANOVA). Differences were considered significant when $P < 0.05$. Quantitative analyses were carried out with GraphPad Prism 7.0 (San Diego, CA, USA). The data and statistical analysis comply with the recommendations of the British Journal of Pharmacology on experimental design and analysis in pharmacology.

2.4 Protein Expression and Purification

The gene encoding BRD4-BD1 with an N-terminal His-tag and a thrombin cleavage site was codon optimized, synthesized and subcloned into the pET-28a expression plasmid. The plasmids were transformed into BL-21 cells and the cells were grown in LB media at 37°C until OD_{600} reached 0.6. Then the cells were induced with 0.2 mM IPTG overnight at 22°C. The cells were collected and resuspended in Buffer A containing 500 mM NaCl, 5 mM imidazole, 5% w/v Glycerol and 50mM HEPES (pH 7.5), and disrupted using a high pressure homogenizer (ATS Engineering), followed by 10 mins of centrifugation at 20,000*g* to remove cell debris. The supernatant was loaded onto a Ni-NTA (Qiagen) column pre-equilibrated with buffer A. The column was washed with 25 mL of the same buffer containing 50mM imidazole in order to remove non-specific bound protein. His-tagged BRD4 BD1 was eluted with buffer B (500 mM NaCl, 250 mM imidazole, 5% w/v Glycerol, 50mM HEPES, pH 7.5). The peak fractions from the Ni-NTA column were pooled and cleaved with thrombin overnight at 4 °C. The cleaved BRD4 BD1 was further purified with a Superose 12

gel filtration column (GE Healthcare) and concentrated to 7 mg/mL. The expression and purification of BRD4 BD2 was essentially the same as BD1, except a TEV cleavage site was inserted between the His-tag and the target gene, and the Ni-NTA column purified BD2 protein was cleaved with TEV protease.

Crystallization was performed by using the sitting drop vapor diffusion method. For BD1, 1 μL solution containing 7 mg/mL of protein in 20 mM Trisand 50 mM NaCl (pH 8.0), was mixed with 1 μL of well solution containing 4.0 M sodium formate and 200 mM NDSB-201, with microseeding of native BRD4 BD1 crystal seeds. The crystallization drop was incubated against 50 μL of well solution at 295 K. Crystals appeared in 12 hours and reached the maximum size in 2 days. For BD2, 1 μL protein solution containing 10 mg/mL of protein in 20 mM Tris and 50 mM NaCl (pH 8.0), was mixed with 1 μL of well solution containing 20% v/v polyethylene glycol monomethyl ether 2000 and 100 mM Tris (pH 8.5) and incubated against 50 μL of well solution at 295 K. BD2 crystals appeared in 12 hours and reached the maximum size in 24 hours. Protein-compound complex crystals were obtained by soaking the native crystals in a solution containing the same well solution supplemented with some granules of the compound.

BD1-**3478** crystals were transferred to a cryoprotectant solution comprising 4.0 M sodium formate and 20% glycerol, and BD2-**3478** crystals were transferred to a cryoprotectant solution comprising 27% v/v polyethylene glycol monomethyl ether 2000 and 100 mM Tris (pH 8.5), then the cryo protected crystals were flash-frozen in

liquid nitrogen. X-ray data of each protein−compound complex were collected from a single crystal at 100 K at BL17U1 of Shanghai Synchrotron Radiation Facility. Images were processed with Mosflm (Battye, Kontogiannis, Johnson, Powell & Leslie, 2011). BD1 crystals belong to space group $P2_12_12_1$ and BD2 crystals belong to the space group $P22_12_1$（Table 1）.

The structures of protein−compound complexes were solved by molecular replacement implemented in Phaser (McCoy, Grosse-Kunstleve, Adams, Winn, Storoni & Read, 2007). Coordinates of BD1 (PDB ID code 4PCE) and BD2 (PDB ID code 6C7Q) were used as the original search models. The structure models of the compound were manually fit in the electron density using COOT (Emsley, Lohkamp, Scott & Cowtan, 2010). The built models were refined by the program PHENIX. Figures of protein structures were created with Pymol (http://www.pymol.org). The coordinates for the models of BRD4-BD1 and BRD4-BD2 have been deposited in the Protein Data Bank, https://www.rcsb.org (PDB ID codes 7C2Z and 7C6P).

Table 1. Data collection statistics for crystals of BD1-**3478** and BD2-**3478** complexs. Values shown in parentheses are for the highest resolution shell and data are from a single crystal only.

Property	**Value**	
	BD1-3478 complex	**BD2-3478 complex**
Space group	$P\ 2_12_12_1$	$P\ 2\ 2_1\ 2_1$
Cell constants a, b, c	32.23 Å 47.22 Å 79.56 Å	33.59 Å 63.01 Å 70.50 Å

Resolution (Å)	40.61-1.30（1.32-1.30）	35.25-1.73（1.76-1.73）
% Data completeness	86.0 (87.1)	99.9 (100)
R_{merge}	0.089（0.120）	0.079（0.138）
$< I/\sigma(I) >$ [1]	4.4 (1.0)	6.3 (1.0)
$CC_{1/2}$	0.991（0.533）	0.985（0.415）
Redundancy	3.0（3.5）	3.9（5.4）
R_{work}/R_{free}	0.1883/0.1992	0.1893/0.2216

[1] Intensities estimated from amplitudes.

3 RESULTS

3.1 BRD4 is highly overexpressed in AML cancer patients and its level is an indicator of prognosis

By querying Cancer Genome Atlas (TCGA) database（http://gepia.cancer-pku.cn）, we found that in acute myeloid leukemia (LAML) patients, the mRNA expression level of BRD4 in tumors was significantly higher than in normal controls (Fig. 1A). Consistently, we observed higher levels of BRD4 protein abundance in MV4-11 (AML) and MKN45 (gastric cancer) compared with A549 (lung cancer) and HepG2 (liver cancer) cells (Fig. 1B). In addition, an inverse correlation between BRD4 expression and overall survival rate in LAML and ACC cohorts were observed, suggesting that lower BRD4 expression may be associated with a favorable prognosis (Fig. 1C).

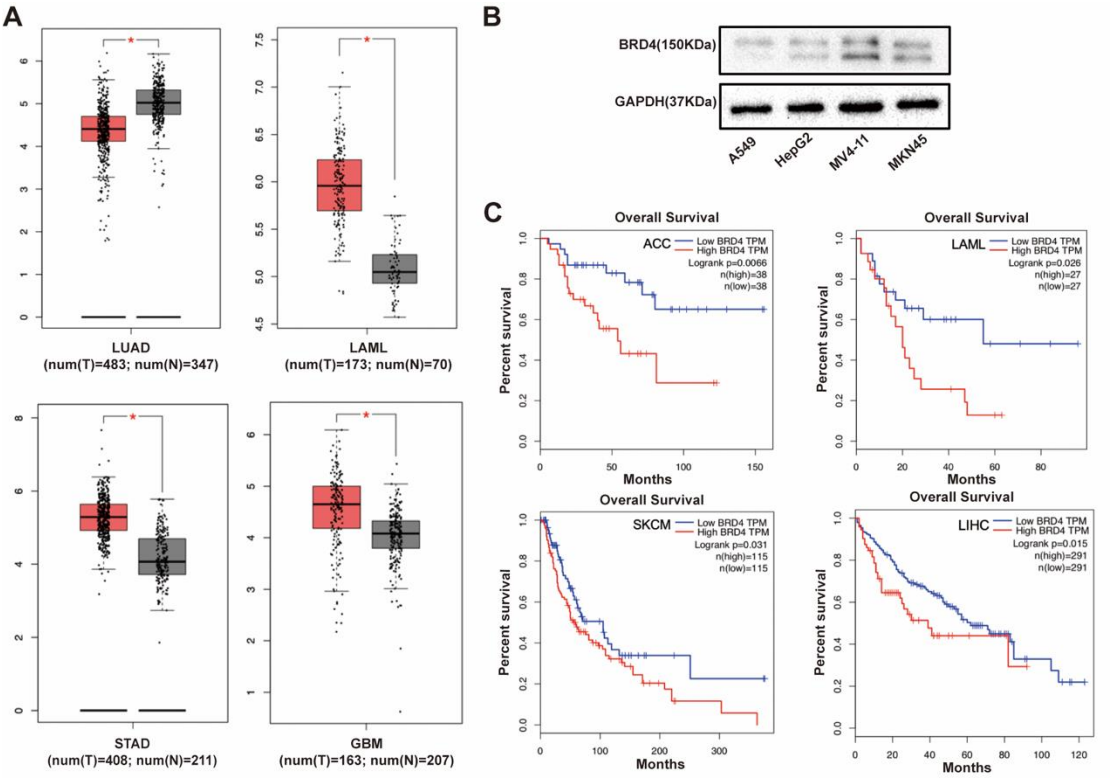

Figure 1. (A). The BRD4 expression levels in four cancers, detected by TIMER (*P<0.05). LUAD, LAML, STAD and GBM stand for lung adenocarcinoma, acute myeloid leukemia, stomach adenocarcinoma and glioblastoma multiforme, respectively. (B). Western blotting analysis of BRD4 expression in A549, HepG2, MV4-11 and MKN45 cell lines. (C). Comparison of Kaplan-Meier survival estimates with respect to BRD4 expression levels in different cancers. Low BRD4 expression levels shown favorable overall survival (OS) in adrenal cortical carcinoma (ACC), LAML, skin cutaneous melanoma (SKCM) and liver hepatocellular carcinoma (LIHC), according to the Kaplan-Meier plotter database.

3.2 AlphaScreen identified 3478 as a potent inhibitor of BRD4

Of the 11 compounds (flavonoids and derivatives) tested with AlphaScreen assay at 10 μM, only **3478** showed apparent inhibition against BRD4-BD1 (Table 2, Fig. 2A).

Then **3478** was further tested with 10 dose IC_{50} AlphaScreen assay against BRD4 BD1 and BD2 to determine the accurate inhibitory activities. Remarkably, **3478** is ~100-fold selective for BD2 (IC_{50} = 2.04 x 10^{-7} M) than BD1 (IC_{50} = 1.80 x 10^{-6} M) (Fig. 2C). The positive control JQ1 showed no significant selectivity. (IC_{50} = 5.53 x 10^{-8}M for BD1 and IC_{50} = 8.99 x 10^{-9}M for BD2) (Fig. 2B).

Table 2. Inhibitory activities of flavonoids and derivatives.

No.	Compound	Chemical structure	(% protein activity in the presence of 10μM compound)
1	Naringenin	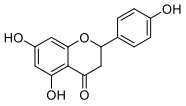	103.50
2	Taxifolin	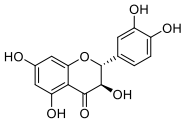	106.08
3	Hesperetin	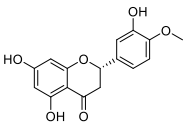	106.01
4	Genistein	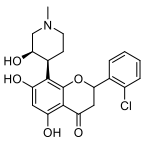	102.01
5	Flavopiridol	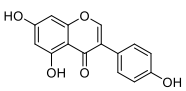	102.56
6	6-Phenyl-3,4-dihydro-2(1h)-one	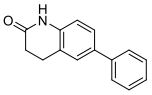	106.80
7	1N-Methyl-6-Phenyl-3,4-dihydro-2(1h)-one	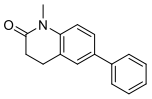	97.35

8	1N-Methyl-7-Phenyl-3,4-dihydro-2(1h)-one	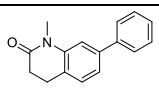	104.97
9	7-Phenyl-3,4-dihydro-2(1h)-one	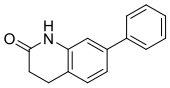	101.44
10	3’,4’,7,8- tetrahydroxyflavanon	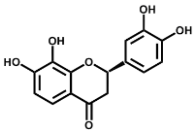	103.78
3478	3’,4’,7,8- tetrahydroxyflavonoid	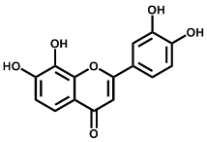	44.68

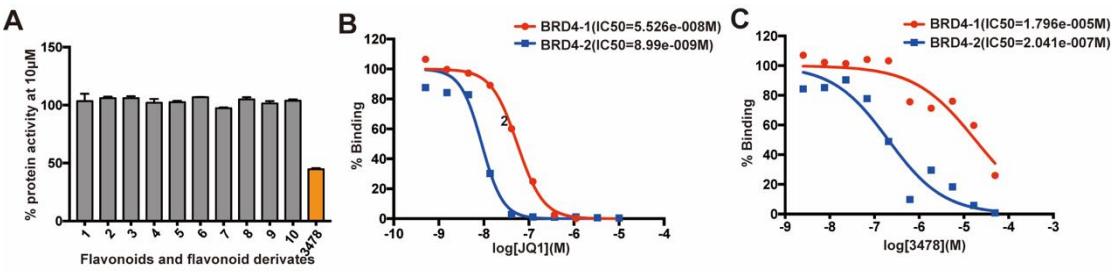

Figure 2. AlphaScreen Binding assays. (A). Inhibitory activities of 10 μM different compounds against BRD4-BD1. (B). 10 dose AlphaScreen assays of JQ1 against BRD4-BD1 and BD2. (C). 10 dose AlphaScreen assays of **3478** against BRD4-BD1 and BD2.

3.3 Crystallographic studies show that 3478 binds to the ligand binding pocket of BD1 or BD2 and His433 of BD2 is responsible for the selectivity

X-ray structures of **3478** in complex with BRD4-BD1 or BD2 were determined at resolution of 1.30Å and 1.73Å (Table 1), respectively. **3478** binds very similarly to BD1 and BD2 in the binding pocket (Fig. 3). In both structures, the carbonyl group of **3478** forms strong H-bonds with an asparagine residue (BD1: N140, BD2: N433), and

a water molecule near the tyrosine residue (BD1: Y97, BD2: Y390). 7-hydroxy of **3478** forms a third H-bond with the main chain carbonyl group of a proline residue (BD1: P82, BD2: P375). These 3 H-bonds fix the 2,3-dihydro-1-benzopyran-4-one ring tightly in the binding pocket. In addition, hydrophobic residues V87, I146, and I94 (BD1) or V380, V439, and L387 (BD2) formed strong hydrophobic interaction with **3478 (**Fig. 3C, D**)**.

In the crystal of BD1-**3478** complex, the weak electron density of the phenyl group of **3478** suggests a weak interaction of this phenyl group with BD1 (Fig. 3A). In contrast, its density is well defined in BD2-**3478** structure (Fig. 3B), suggesting a fixed conformation and stronger interactions in BD2. **3478** forms one additional H-bond with the water molecule near N433, and likely establishes hydrophobic interaction with His437, as NH of His437 points to two carbon atoms in its phenyl ring. The corresponding position of His433 in BD1 is an aspartic acid (D144) whose side chain is too distant from **3478** to establish effective interaction. In a recently published paper, His437 of BD2 is exploited to design inhibitors with selectivity for BD2 (Faivre et al., 2020).

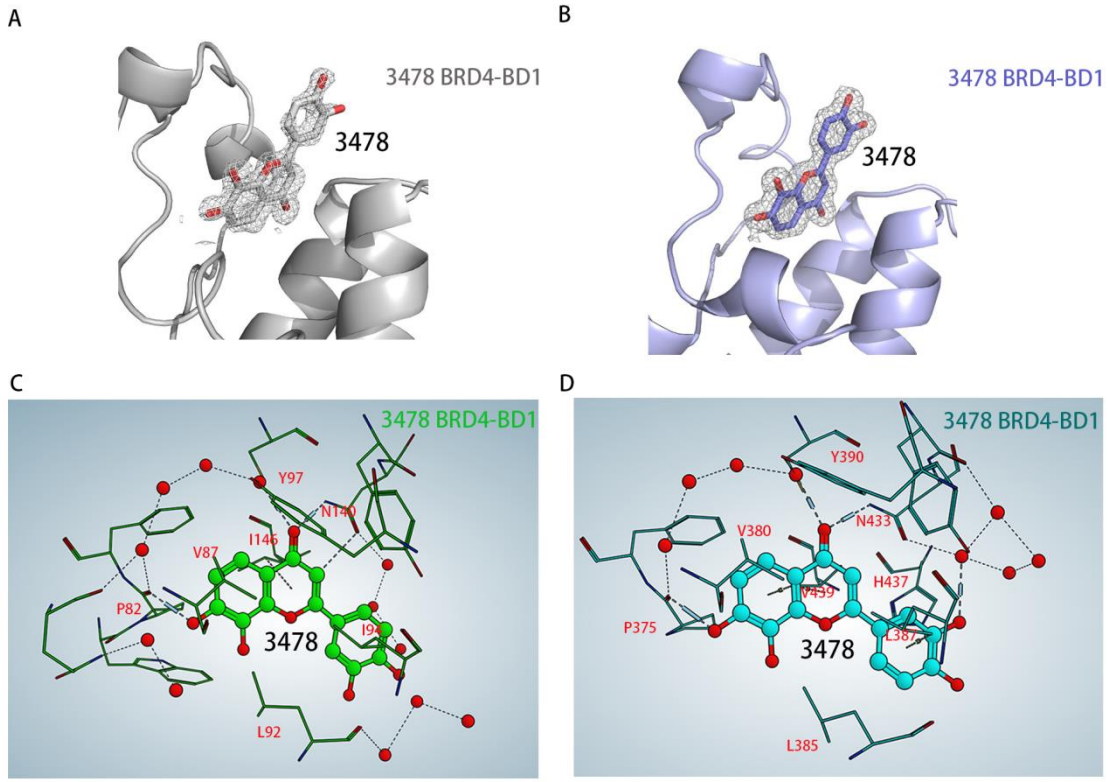

Figure 3. Cartoon representations of the co-crystal structures of BRD4-BD1 (A) and BRD4-BD2 (B) in complex with **3478 (**stick representation**)**. 2Fo-Fc maps were contoured at 2.0 σ. Interactions of **3478** with BRD4-BD1 and **3478** was shown in ball-and-stick, with carbon atoms colored in green and oxygen atoms in red (C). Interactions of **3478** with BRD4-BD2 and **3478** was shown in ball-and-stick, with carbon atoms colored in light blue and oxygen atoms in red (D). Waters were shown as red spheres. The blue cylinder lines represented the H-bonds of the ligand with the protein and the structured waters, and the blue thin lines represented the H-bonds of water with water or water with protein. MOE 2019.01(https://www.chemcomp.com/) analyzed the H-bond network and generated the figures (C, D).

3.4 3478 inhibited MV4-11 cell proliferation and induced apoptosis

JQ1 was used as the positive control as it was one of the most studied BRD4

inhibitors that shown anti-tumor potential for both blood cancers and solid tumors (Leal, Williams, Royce, Pioli, Sporn & Liby, 2017; Zuber et al., 2011). CCK8 assays showed that JQ1 and **3478** inhibited MV4-11 cell growth in a dose- and time-dependent manner. IC_{50} of JQ1 and **3478** were 0.91μM (Fig. 4A) and 30.17 μM (Fig. 4B) after 48 hours, respectively. FACS analysis of double-stained MV4-11 cells with Annexin V-FITC/PI showed that JQ1 or **3478** treatment for 48 hours caused significantly higher apoptosis rates compared with untreated control cells (Fig. 4C, D).

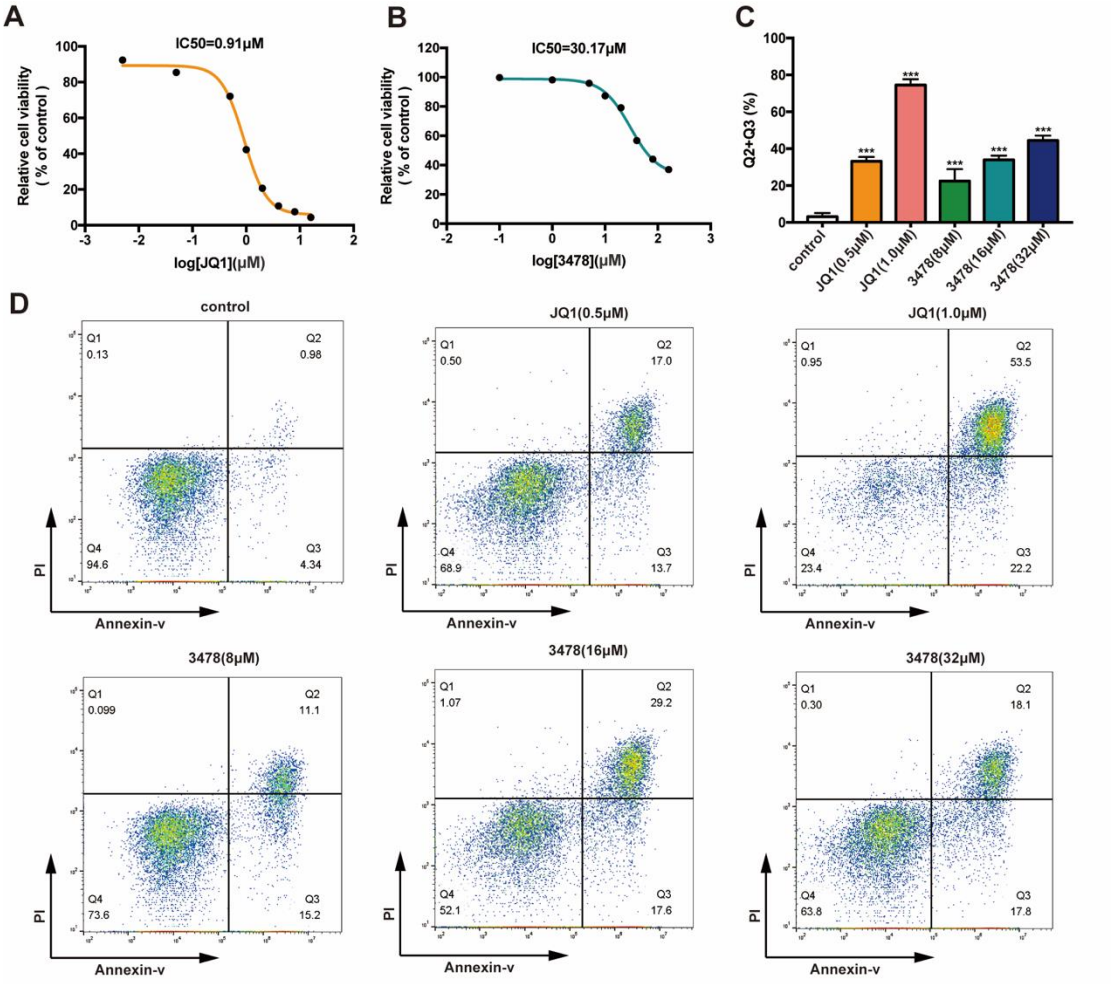

Figure 4. **3478** inhibited MV4-11 cells growth. MV4-11 cells were treated with JQ1 (A). or **3478** (B). for 48h and analyzed by CCK8 kits. The IC_{50} values were calculated

using GraphPad Prism 7.0. (C). The percentages of apoptotic cells (the lower-right quadrant of the FACS histograms (percentage of early apoptotic cells) and the upper-right quadrant (percentage of late apoptotic cells)) were shown. All results were representative images from three experiments. (D). The MV4-11 cells were exposed to different concentrations of JQ1, **3478** or culture medium for 48h and stained with Annexin V-FITC and PI for apoptosis measurement by flow cytometry.

3.5 3478 retarded tumor growth in the MV4-11 xenograft mice model

To evaluate the anti-AML efficacy of **3478** *in vivo*, nude mice bearing subcutaneous MV4-11 xenografts were treated with 50mg/kg or 100mg/kg **3478** once a day for 4 weeks and compared with negative (0.3% CMC-Na treatment daily) and positive (50mg/kg JQ1 treatment daily) controls. The results showed that **3478** effectively inhibited tumor progression (Fig. 5A-C). On day 28, the relative tumor volume was 6.89, 1.03, 3.46 and 2.52 for mice treated with 0.3% CMC-Na, 50mg/kg JQ1, 50mg/kg **3478** and 100mg/kg **3478**, respectively (Fig. 5A), as shown in (Fig. 5C). The average tumor weight on day 28 of 50mg/kg and 100mg/kg **3478** dose groups were 0.68g and 0.39g, while it was 0.79g for model group and 0.22g for JQ1 group (Fig. 5B). In addition, **3478** caused no notable side effects indicated by body weight and visceral index (Fig. 5D, E).

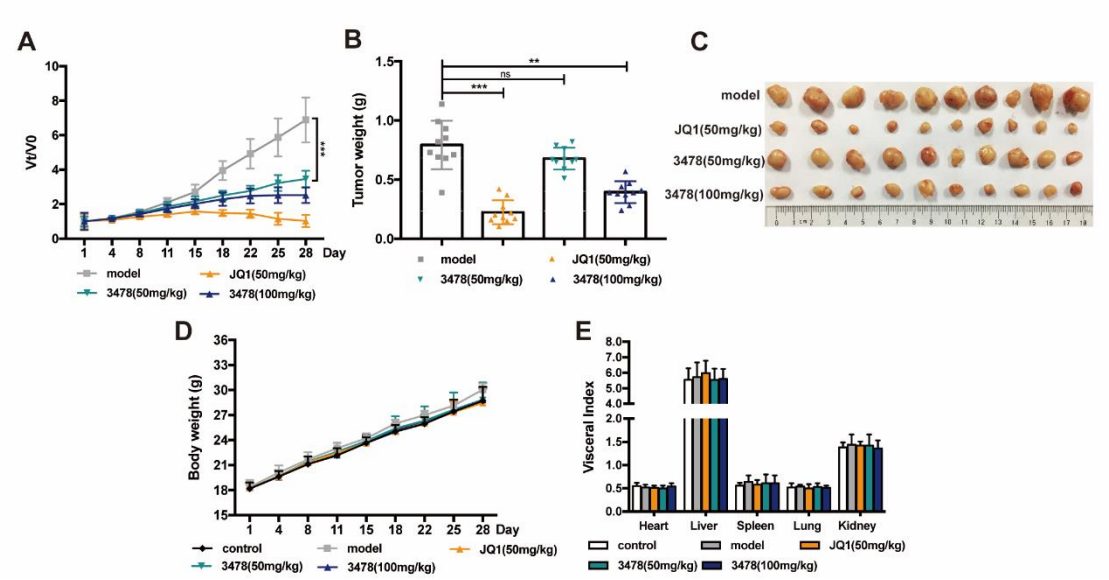

Figure 5. The effect of **3478** on MV4-11-implanted AML tumor *in vivo*. (A). Tumor volumes of mice treated with 0.3% CMC-Na (model), JQ1(50mg/kg), **3478** (50mg/kg), and **3478** (100mg/kg). (B). Weights of tumors from different groups of mice on day 28. (C). Photographs of tumor blocks from different groups on day 28. (D). Body weight changes of mice in different groups at 1, 4, 8, 11, 15, 18, 22, 25, 28 day time points. (E). The visceral index of mice from different groups on day 28 compared with the model group: **P*<0.05, ***P*<0.01, ****P*<0.001.

3.6 3478 suppressed AML progression through regulating BRD4/c-Myc signaling pathway

C-Myc is a downstream target activated by BRD4, which affects cell proliferation. To identify the signaling pathway responsible for **3478**-induced inhibition of cell growth, we performed Western blotting and RT-qPCR assays to examine the mRNA and protein expression levels of related proteins *in vitro*. Our results showed that the level of BRD4 protein was not influenced by **3478** treatment (Fig. 6A). As expected, **3478**

down-regulated c-Myc expression at both mRNA and protein levels as JQ1 did (Wang et al., 2018) (Fig. 6A, B). Consistent with the results *in vitro*, **3478** treatment reduced c-Myc expression at both mRNA and protein levels in MV4-11 xenograft mice (Fig. 6C, D). Immunofluorescence assay of tumor samples also showed that **3478** treatment inhibited c-Myc expression in nucleus and cytoplasm (Fig. 6E). Collectively, these results indicate that **3478** targets BRD4-driven oncogenic pathways with increased c-Myc expression.

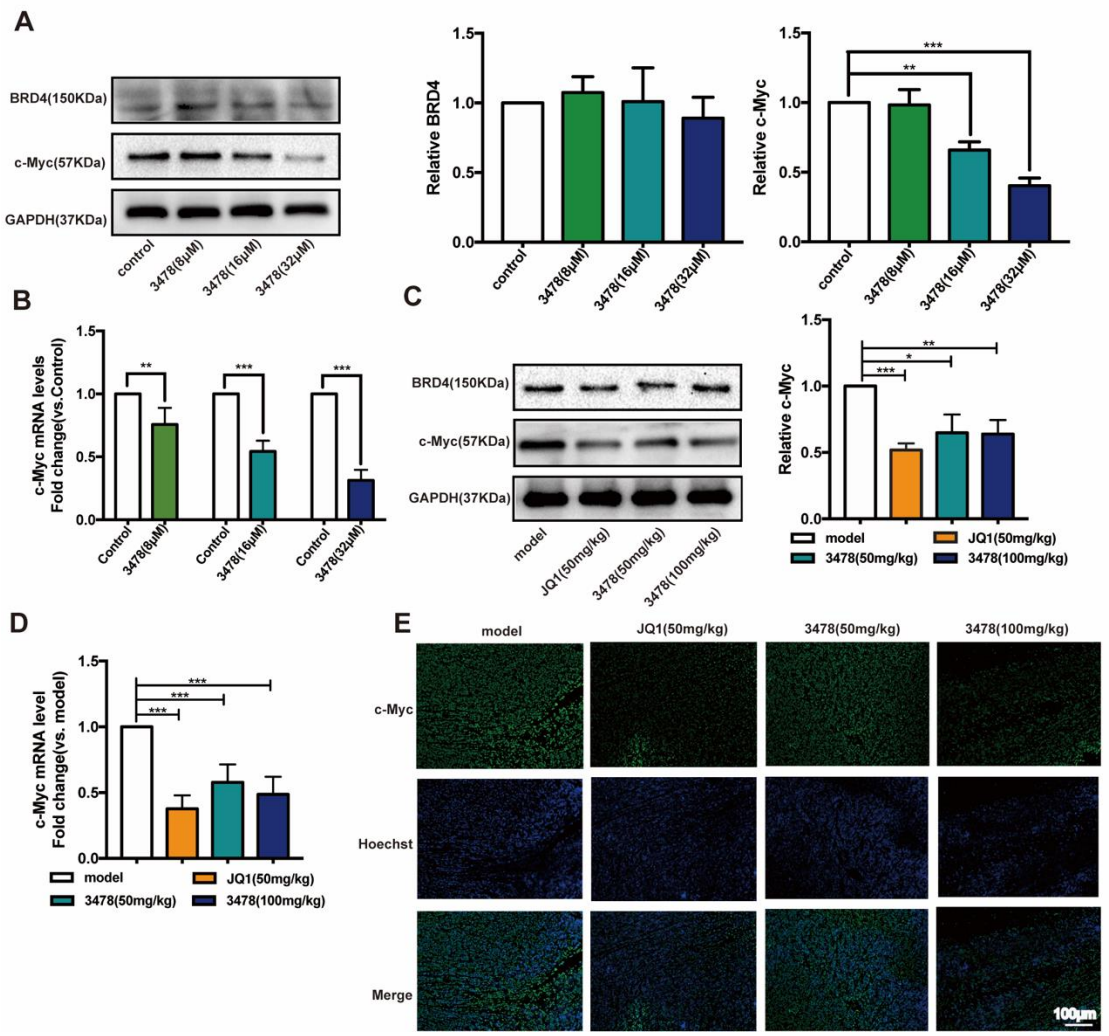

Figure 6. Compound **3478** downregulated the c-Myc both in MV4-11 cells and MV4-11 xenograft tumors through BRD4/c-Myc signaling pathway. (A). The protein

expression of BRD4 and c-Myc after **3478** treatment were measured by Western blotting. Quantification of protein level was normalized to GAPDH using densitometry. (B). The mRNA level of c-Myc in MV4-11 cells after **3478** intervention was determined by real-time qPCR. GAPDH was used as the loading control. (C). The protein expression of BRD4 and c-Myc in MV4-11 xenograft tumors in the different groups were measured by Western blotting. Quantification of protein level was normalized to GAPDH using densitometry. (D) The mRNA level of c-Myc in MV4-11 xenograft tumors in the different groups were determined by RT-qPCR. GAPDH was used as the loading control. (E). Immunofluorescence analysis of c-Myc localization and expression in MV4-11 transplanted tumor tissues in different groups (100×, scale bar represented 100μm). Compared with control or model group: **P*<0.05, ***P*<0.01, ****P*<0.001. Data in panels represented means ± SD from 10 animals. Independent experiments were performed in triplicate.

4 DISCUSSION

BRD4 is the most extensively studied BET family member, which is the epigenetic reader of histone code. It recruits transcriptional regulator complexes to chromatin and binds to acetylated lysine (KAc) residues on the N-terminal tails of histones to activate RNA polymerase II. Due to its central role in cell proliferation, apoptosis and transcription, BRD4 is considered a promising drug target for a number of human diseases including cancer, inflammation and cardiovascular diseases. Inhibiting BRD4 displays efficacy against diseases especially cancer and inflammation. Therefore, discovery of high potency and low toxic BRD4 inhibitors attracts huge interest from

medical chemists.

Flavonoids are a kind of ubiquitous natural products in plants and essential active ingredients of many medicinal plants. They have the characteristics of broad biological activity, high efficiency and are generally considered safe, with good prevention and cure effects on various types of tumors (Kashyap et al., 2019). Previous studies show flavonoids can inhibit occurrence and development of cancer in various aspects, including the inhibition of aerobic glycolysis, the promotion of apoptosis, the retardation of cell cycle, the suppression of invasion and migration, the induction of DNA damage, and the inhibition of aromatase and microtubule production (Pang, Chu & Yang, 2018). In this study, we discovered 3',4',7,8-tetrahydroxyflavonoid, a natural flavonoid found in Acacia burkittii and Acacia acuminata Heartwoods(Grace, Wilsonb, Kandil, Dimitriadis & Coates, 2009), can potently inhibit BRD4-BD2 with ~100 folds selectivity of BRD4-BD1. The inhibitory activity to BRD4 is not a common feature of flavonoid, as the other 11 flavonoid compounds showed no apparent inhibition to BRD4-BD1 at the concentration of 10 μM, suggesting the positions of hydroxyl groups are critical to the inhibitory activity. In addition, an aromatic heterocyclic C ring is important for the inhibitory activity, for 3′,4′,7,8-tetrahydroxyflavonoide, the hydrogenated derivative of **3478**, loses inhibitory activity to BRD4-BD1. The importance of the hydroxyl group positions is confirmed by co-crystal structure of **3478** in complex with BRD4-BD1 and BD2, in which the compound forms hydrogen bonds with the proteins by its hydroxyl group. The crystal structures suggest that the selectivity is mainly due to the two extra

hydrogen bonds and the hydrophobic interaction between Histidine 477 of BD2 and phenyl group of **3478**. The chemical scaffold of **3478** and its binding mode with BRD4 bromodomains are distinctively different from the reported BRD4 inhibitors to date. To evaluate the efficacy of **3478** *in vivo*, we constructed MV4-11 mouse xenograft model and the results showed that **3478** had a dose-dependent inhibitory activity: at 50 mg/kg dose, the size of tumor was significantly smaller compared with the negative control group, and at 100 mg/kg dose, the size of tumor was comparable to that treated with 50 mg/kg JQ1. No noticeable body weight loss was observed upon the treatment of 100 mg/kg **3478**, suggesting its low toxicity. Western blotting results showed that compound **3478** remarkably reduced the c-Myc expression at mRNA and protein levels, while BRD4 level remained unchanged.

The protooncogene c-Myc is a key regulator of hyperproliferation, cell cycle progression and metastasis, which is essential for lymphoid (de Alboran et al., 2001; Douglas, Jacobs, Bothwell & Hayday, 2001) and megakaryocytic/erythroid development (Guo et al., 2009). The epigenetic regulation at the c-Myc locus plays a critical role in myeloid differentiation and leukemia. The BRD4 and SWI/SNF complexes regulate c-Myc expression from the distal super-enhancer BDME (BRD4-dependent c-Myc enhancer), 1.7 megabases (Mb) downstream from its transcription start site (TSS, (Shi et al., 2013; Yashiro-Ohtani et al., 2014)). Disrupting the protein−protein interactions between BRD4 and acetyl-lysine can effectively repress the transcription of c-Myc oncogene and c-Myc dependent genes and inhibit the proliferation of cancer cells such as AML, the activated B-cell-like subtype (ABC)

of diffuse large B-cell lymphoma (DLBCL) (Ceribelli et al., 2014; Chapuy et al., 2013; Takimoto-Shimomura et al., 2019), neuro-blastoma (Puissant et al., 2013), and lung adenocarcinoma (Lockwood, Zejnullahu, Bradner & Varmus, 2012). Therefore, BRD4 has become a promising anti-cancer drug target that attracts huge interest in discovering BRD4 inhibitors (Delmore et al., 2011).

In conclusion, we discovered a natural product, **3478**, as a potent inhibitor of BRD4 with a novel chemical scaffold and binding mode to BRD4 with ~100-fold selectivity for BRD4-BD2 (IC_{50} = 2.04 x 10^{-7} M). The compound can effectively inhibit the growth of MV4-11 tumor size in a mouse xenograft model and reduce the c-Myc level. Its anti-cancer activity provides solid scientific rationale for its application in cancer treatment. Considering its high potency, selectivity for BD2, its small size (molecular weight = 286) and novel chemical scaffold, it is worth to be explored as a lead compound to inspire anti-cancer drug design and to treat other BRD4-related diseases.

ACKNOWLEDGEMENTS

We thank staff from the Experiment Center for Science and Technology of Nanjing University of Chinese Medicine, and the Shanghai Synchrotron Radiation Facility (SSRF) beamline BL17U1 for their support. This work was funded by National Key R & D Plan for Precision Medicine Research (Grant 2016YFC0905900), the Priority Academic Program Development of Jiangsu Higher Education Institutions (Integration of Chinese and Western Medicine), Postgraduate Practice Innovation Program of Jiangsu Province 021093002283 (to J. L.).

AUTHOR CONTRIBUTIONS

J. L. and J. Z. designed research; J. L. and W. Z. performed research; and all authors analyzed data and wrote the paper.

CONFLICT OF INTEREST STATEMENT

The authors declare no competing interests.

DECLARATION OF TRANSPARENCY AND SCIENTIFIC RIGOUR

This Declaration acknowledges that this paper adheres to the principles for transparent reporting and scientific rigour of preclinical research as stated in the BJP guidelines for Design & Analysis, Immunoblotting and Immunochemistry, and Animal Experimentation, and as recommended by funding agencies, publishers, and other organizations engaged with supporting research.

REFERENCES

Amorim S, Stathis A, Gleeson M, Iyengar S, Magarotto V, Leleu X*, et al.* (2016). Bromodomain inhibitor OTX015 in patients with lymphoma or multiple myeloma: a dose-escalation, open-label, pharmacokinetic, phase 1 study. The Lancet Haematology 3**:** e196-204.

Battye TG, Kontogiannis L, Johnson O, Powell HR, & Leslie AG (2011). iMOSFLM: a new graphical interface for diffraction-image processing with MOSFLM. Acta Crystallogr D Biol Crystallogr 67**:** 271-281.

Ceribelli M, Kelly PN, Shaffer AL, Wright GW, Xiao W, Yang Y*, et al.* (2014). Blockade of oncogenic IkappaB kinase activity in diffuse large B-cell lymphoma by bromodomain and extraterminal domain protein inhibitors. Proceedings of the National Academy of Sciences of the United States of America 111**:** 11365-11370.

Chapuy B, McKeown MR, Lin CY, Monti S, Roemer MG, Qi J*, et al.* (2013). Discovery and characterization of super-enhancer-associated dependencies in diffuse large B cell lymphoma. Cancer Cell 24**:** 777-790.

de Alboran IM, O'Hagan RC, Gärtner F, Malynn B, Davidson L, Rickert R*, et al.* (2001). Analysis of

C-MYC function in normal cells via conditional gene-targeted mutation. Immunity 14: 45-55.

Delmore JE, Issa GC, Lemieux ME, Rahl PB, Shi J, Jacobs HM, *et al.* (2011). BET bromodomain inhibition as a therapeutic strategy to target c-Myc. Cell 146: 904-917.

Douglas NC, Jacobs H, Bothwell AL, & Hayday AC (2001). Defining the specific physiological requirements for c-Myc in T cell development. Nature immunology 2: 307-315.

Drewry DH, & Macarron R (2010). Enhancements of screening collections to address areas of unmet medical need: an industry perspective. Current opinion in chemical biology 14: 289-298.

Emsley P, Lohkamp B, Scott WG, & Cowtan K (2010). Features and development of Coot. Acta Crystallogr D Biol Crystallogr 66: 486-501.

Eriksson A, Cao R, Pawliuk R, Berg SM, Tsang M, Zhou D, *et al.* (2002). Placenta growth factor-1 antagonizes VEGF-induced angiogenesis and tumor growth by the formation of functionally inactive PlGF-1/VEGF heterodimers. Cancer Cell 1: 99-108.

Faivre EJ, McDaniel KF, Albert DH, Mantena SR, Plotnik JP, Wilcox D, *et al.* (2020). Selective inhibition of the BD2 bromodomain of BET proteins in prostate cancer. Nature 578: 306-310.

Filippakopoulos P, & Knapp S (2014). Targeting bromodomains: epigenetic readers of lysine acetylation. Nature reviews Drug discovery 13: 337-356.

Filippakopoulos P, Picaud S, Mangos M, Keates T, Lambert JP, Barsyte-Lovejoy D, *et al.* (2012). Histone recognition and large-scale structural analysis of the human bromodomain family. Cell 149: 214-231.

Filippakopoulos P, Qi J, Picaud S, Shen Y, Smith WB, Fedorov O, *et al.* (2010). Selective inhibition of BET bromodomains. Nature 468: 1067-1073.

Gilan O, Rioja I, Knezevic K, Bell MJ, Yeung MM, Harker NR, *et al.* (2020). Selective targeting of BD1 and BD2 of the BET proteins in cancer and immunoinflammation. Science (New York, NY) 368: 387-394.

Grace MH, Wilsonb GR, Kandil FE, Dimitriadis E, & Coates RM (2009). Characteristic flavonoids from Acacia burkittii and A. acuminata heartwoods and their differential cytotoxicity to normal and leukemia cells. Natural product communications 4: 69-76.

Guo Y, Niu C, Breslin P, Tang M, Zhang S, Wei W, *et al.* (2009). c-Myc-mediated control of cell fate in megakaryocyte-erythrocyte progenitors. Blood 114: 2097-2106.

Hert J, Irwin JJ, Laggner C, Keiser MJ, & Shoichet BK (2009). Quantifying biogenic bias in screening libraries. Nature chemical biology 5: 479-483.

Hosaka K, Yang Y, Seki T, Nakamura M, Andersson P, Rouhi P, *et al.* (2013). Tumour PDGF-BB expression levels determine dual effects of anti-PDGF drugs on vascular remodelling and metastasis. Nature communications 4: 2129.

Kashyap D, Garg VK, Tuli HS, Yerer MB, Sak K, Sharma AK, *et al.* (2019). Fisetin and Quercetin: Promising Flavonoids with Chemopreventive Potential. Biomolecules 9.

Kilkenny C, Browne WJ, Cuthill IC, Emerson M, & Altman DG (2010). Improving bioscience research reporting: the ARRIVE guidelines for reporting animal research. PLoS Biol 8: e1000412.

Leal AS, Williams CR, Royce DB, Pioli PA, Sporn MB, & Liby KT (2017). Bromodomain inhibitors, JQ1 and I-BET 762, as potential therapies for pancreatic cancer. Cancer letters 394: 76-87.

Liu Z, Wang P, Chen H, Wold EA, Tian B, Brasier AR, *et al.* (2017). Drug Discovery Targeting Bromodomain-Containing Protein 4. J Med Chem 60: 4533-4558.

Lockwood WW, Zejnullahu K, Bradner JE, & Varmus H (2012). Sensitivity of human lung adenocarcinoma cell lines to targeted inhibition of BET epigenetic signaling proteins. Proceedings of the National Academy of Sciences of the United States of America 109: 19408-19413.

McCoy AJ, Grosse-Kunstleve RW, Adams PD, Winn MD, Storoni LC, & Read RJ (2007). Phaser crystallographic software. J Appl Crystallogr 40: 658-674.

Morinière J, Rousseaux S, Steuerwald U, Soler-López M, Curtet S, Vitte AL, *et al.* (2009). Cooperative binding of two acetylation marks on a histone tail by a single bromodomain. Nature 461: 664-668.

Muller S, Filippakopoulos P, & Knapp S (2011). Bromodomains as therapeutic targets. Expert reviews in molecular medicine 13: e29.

Pang BB, Chu YK, & Yang H (2018). [Anti-breast cancer mechanism of flavonoids]. Zhongguo Zhong yao za zhi = Zhongguo zhongyao zazhi = China journal of Chinese materia medica 43: 913-920.

Piha-Paul SA, Sachdev JC, Barve M, LoRusso P, Szmulewitz R, Patel SP, *et al.* (2019). First-in-Human Study of Mivebresib (ABBV-075), an Oral Pan-Inhibitor of Bromodomain and Extra Terminal Proteins, in Patients with Relapsed/Refractory Solid Tumors. Clinical cancer research : an official journal of the American Association for Cancer Research 25: 6309-6319.

Puissant A, Frumm SM, Alexe G, Bassil CF, Qi J, Chanthery YH, *et al.* (2013). Targeting MYCN in neuroblastoma by BET bromodomain inhibition. Cancer Discov 3: 308-323.

Sheppard GS, Wang L, Fidanze SD, Hasvold LA, Liu D, Pratt JK, *et al.* (2020). Discovery of

N-Ethyl-4-[2-(4-fluoro-2,6-dimethyl-phenoxy)-5-(1-hydroxy-1-methyl-ethyl)phenyl]-6-methyl-7-oxo-1H-pyrrolo[2,3-c]pyridine-2-carboxamide (ABBV-744), a BET Bromodomain Inhibitor with Selectivity for the Second Bromodomain. J Med Chem 63**:** 5585-5623.

Shi J, Whyte WA, Zepeda-Mendoza CJ, Milazzo JP, Shen C, Roe JS*, et al.* (2013). Role of SWI/SNF in acute leukemia maintenance and enhancer-mediated Myc regulation. Genes & development 27**:** 2648-2662.

Shin DG, & Bayarsaihan D (2017). A Novel Epi-drug Therapy Based on the Suppression of BET Family Epigenetic Readers. The Yale journal of biology and medicine 90**:** 63-71.

Takimoto-Shimomura T, Tsukamoto T, Maegawa S, Fujibayashi Y, Matsumura-Kimoto Y, Mizuno Y*, et al.* (2019). Dual targeting of bromodomain-containing 4 by AZD5153 and BCL2 by AZD4320 against B-cell lymphomas concomitantly overexpressing c-MYC and BCL2. Invest New Drugs 37**:** 210-222.

Wang J, Liu Z, Wang Z, Wang S, Chen Z, Li Z*, et al.* (2018). Targeting c-Myc: JQ1 as a promising option for c-Myc-amplified esophageal squamous cell carcinoma. Cancer letters 419**:** 64-74.

Wang Q, Li Y, Xu J, Wang Y, Shi D, Liu L*, et al.* (2019). Computational study on the selective inhibition mechanism of MS402 to the first and second bromodomains of BRD4. Proteins 87**:** 3-11.

Yashiro-Ohtani Y, Wang H, Zang C, Arnett KL, Bailis W, Ho Y*, et al.* (2014). Long-range enhancer activity determines Myc sensitivity to Notch inhibitors in T cell leukemia. Proceedings of the National Academy of Sciences of the United States of America 111**:** E4946-4953.

Zuber J, Shi J, Wang E, Rappaport AR, Herrmann H, Sison EA*, et al.* (2011). RNAi screen identifies Brd4 as a therapeutic target in acute myeloid leukaemia. Nature 478**:** 524-528.